Overview and Commissioning Status of the UCLA MITHRA Facility

Oliver Williams [1,*], Atsushi Fukasawa [1], Yusuke Sakai [1], Gerard Andonian [1], Fabio Bosco [1], Martina Carillo [2], Pratik Manwani [1], Sean O'Tool [1], Jessica Pan [1], Monika Yadav [1] and James Rosenzweig [1]

[1] Department of Physics and Astronomy, University of California, Los Angeles, CA 90095, USA; fuka@g.ucla.edu (A.F.); yusuke@physics.ucla.edu (Y.S.); gerard@physics.ucla.edu (G.A.); fbosco@physics.ucla.edu (F.B.); pkmanwani@gmail.com (P.M.); sean.otool2020@gmail.com (S.O.); jessicayqpan@gmail.com (J.P.); yadavmonika@g.ucla.edu (M.Y.); rosen@physics.ucla.edu (J.R.)

[2] Department of Physics, Sapienza University of Rome, 00185 Rome, Italy; martina.carillo@uniroma1.it

[*] Correspondence: obw@physics.ucla.edu

Abstract: Presented here are the first results of commissioning of the S-Band hybrid photoinjector and laser systems at the new accelerator and light source facility, MITHRA, at UCLA. The radiation bunker and capabilities of the facility are described with motivation for detailed measurement of beam parameters explained. Following thorough characterization of the photoinjector, a 1.5 m linac is to be installed and experiments up to 30 MeV will begin. These will include experiments in basic plasma physics, space plasma, terahertz production in dielectric structures, and inverse Compton scattering and applications for the X-rays produced.

Keywords: photoinjector; terawatt; wakefield; X-ray; terahertz; THz; laser; plasma

1. Introduction

As a university lab, MITHRA serves as an educational and research facility dedicated to the development of future scientists in the areas of advanced accelerators, light sources, and their applications. It is the physical culmination of decades of research efforts of the Particle Beam Physics Lab (PBPL) at UCLA. PBPL has led collaborations with multiple institutions around the world, with a focus on: high gradient RF structures; electron beam interactions with plasmas, lasers, and dielectrics; free electron lasers; high harmonic generation; and advanced beam dynamics.

While the final design of MITHRA includes components not yet installed, and is undoubtedly expected to change with technological advancements, the current vision will enable training and research in the topics mentioned above. The facility therefore has planned many capabilities, including an 80 MeV electron beam in a multi-beamline radiation vault, terawatt laser system with transport into the bunker, cryogenic cooling for advanced high gradient structures, high power RF in C-band and S-band, and various plasma sources.

Commissioning of the facility infrastructure is underway and is reported in the following sections. Measured electron beam and laser parameters and efforts to install additional diagnostics are described. First experiments and applications following the mid-energy upgrade to 30 MeV are discussed and the concept shown for the final 80 MeV design.

2. MITHRA Facility Infrastructure

2.1. Photoinjector Drive Laser

Photoelectrons are produced from the copper cathode in the hybrid gun using 267 nm from a frequency tripled, 800 nm system. This system, a custom Astrella built by Coherent, is a compact, all-in-one laser oscillator, stretcher–compressor, and regenerative amplifier. After the seed from the oscillator is stretched, it is amplified to over 7 mJ, after which 15%

is split off before the compressor and used to seed the terawatt amplifier. The remaining energy is sent to the compressor, where over 5 mJ in 35 fs of IR is then sent to an inline frequency tripling converter, resulting in 350 uJ of UV before the 26 m, in-vacuum transport and spatial filtering. To start, a simple, bulk, polished 10 cm long fused silica rod is used to stretch the UV to approximately 1–2 ps. While continuous, fine control of the cathode laser pulse length using a prism or grating stretcher might eventually be useful for optimization, the beam parameters can be mostly achieved using different lengths of dispersive glass. This has the benefit of preserving laser energy for the cathode as losses in UV pulse stretchers is commonly 70–80%. Currently, after transport losses, over 150 uJ is available for the photocathode.

2.2. Terawatt Laser

The approximately 1 mJ of stretched IR that was split from the drive laser before compression is sent to seed a four-pass, bowtie amplifier, the Hidra-100 system, also built by Coherent. The Ti:Sapphire crystal is pumped by a Continuum Powerlite DLS-8000, providing over 450 mJ of 532 nm at 10 Hz. After the amplified IR passes through a vacuum-compatible, grating-based pulse compressor, over 120 mJ in 35 fs is available for experiments. The high-power laser transport line into the bunker is currently in design and installation is expected in 2024. When installed, the transport line and compressor will exist in vacuum and be connected to the beamline for beam-laser interaction experiments.

2.3. Accelerator

The radiation bunker consists of four-foot-thick concrete walls and ceiling, with a five-foot-thick floor, under which resides the Large Plasma Device, a part of the Basic Plasma Science Facility. The internal dimensions of the bunker are approximately 5 m × 18 m, allowing for multiple experimental beamlines. A typical maze entrance exists as well as a large, mechanized, shielded door to allow for movement of oversized equipment. Penetrations for waveguide, cable, and laser transport are strategically placed through the walls and ceiling.

Directly outside the bunker doors sits the klystron gallery. Two S-band, 25 MW XK-5 klystrons drive the full accelerator, with in-house-built, line-type modulators providing power. Ample electrical and cooling infrastructure exists for magnet power supplies, plasma sources, cryogenics, and to power future RF upgrades at C-band over 25 MW. Collaborative efforts in developing cryogenic S-band and C-band structures are currently underway [1,2], with high energy gain testing to be conducted in the MITHRA bunker. The radiation bunker and a photo of the gallery with installed modulator and klystron is shown in Figure 1 below.

(**a**)　　　　　　　　　　　　　　　　　　(**b**)
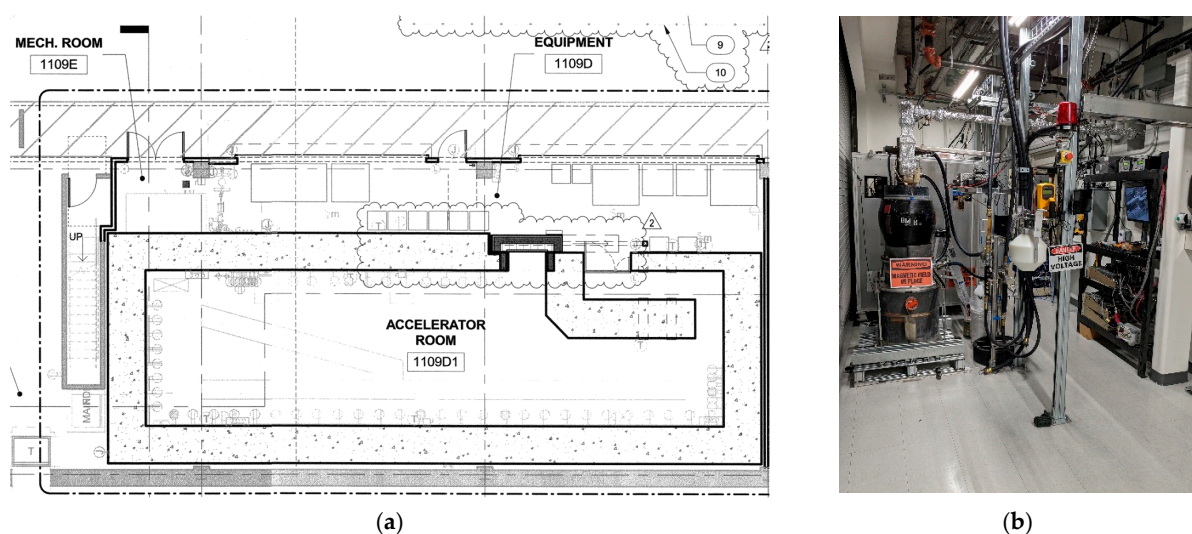
Figure 1. (**a**) Drawing of radiation bunker depicting klystron gallery and accelerator housing; (**b**) photo of klystron gallery with first 25 MW XK-5 and modulator installed.

An S-band hybrid photoinjector provides high brightness and high peak current electron beams before being accelerated at stages; first to 30 MeV and then to 80 MeV. This unique photoinjector design, shown in Figure 2, allows for high peak current beams without the need for magnetic chicane compression or an RF isolator between the klystron and photoinjector, a benefit of pairing the two cavity designs.
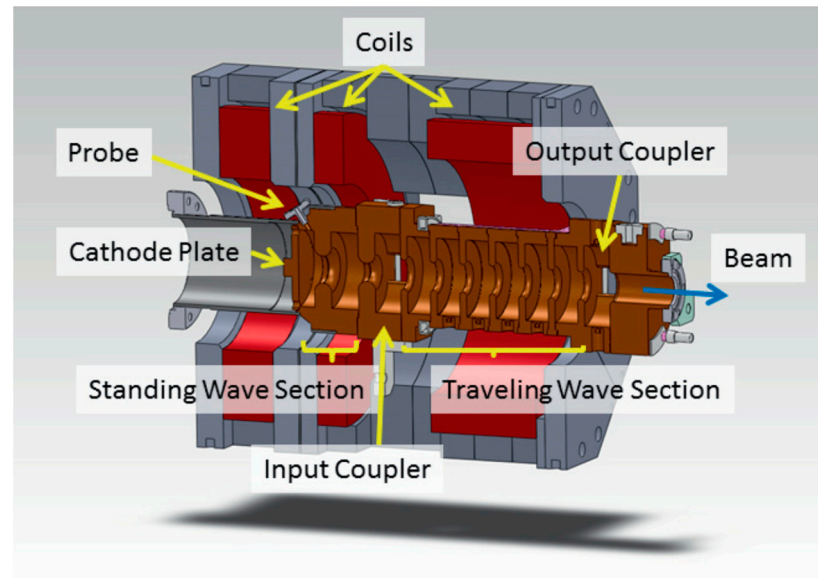
Figure 2. Three-dimensional CAD cross-section of the S-band hybrid gun [3].

The 'hybrid' aspect is due to the existence of both a standing wave accelerating section, as is standard in, for example, the BNL/SLAC/UCLA 1.6 cell gun [4], and a travelling wave section. As the standing wave section fills, RF power starts to propagate into the travelling wave section, where there is a 90-degree phase advance. This results in an electron bunch being launched from the cathode in the standing wave section, then into the travelling wave, where it experiences an energy chirp and subsequent velocity bunching instead of energy gain [5–7]. The phase space is uncorrelated at maximum compression of the electron bunch, approximately 1.5 m from the cathode, where the entrance to the linac will be placed. The relationship between injection phase, energy spread, and velocity bunching can be seen in Figure 3, as generated by the code GPT (General Particle Tracer).

(**a**)   (**b**)
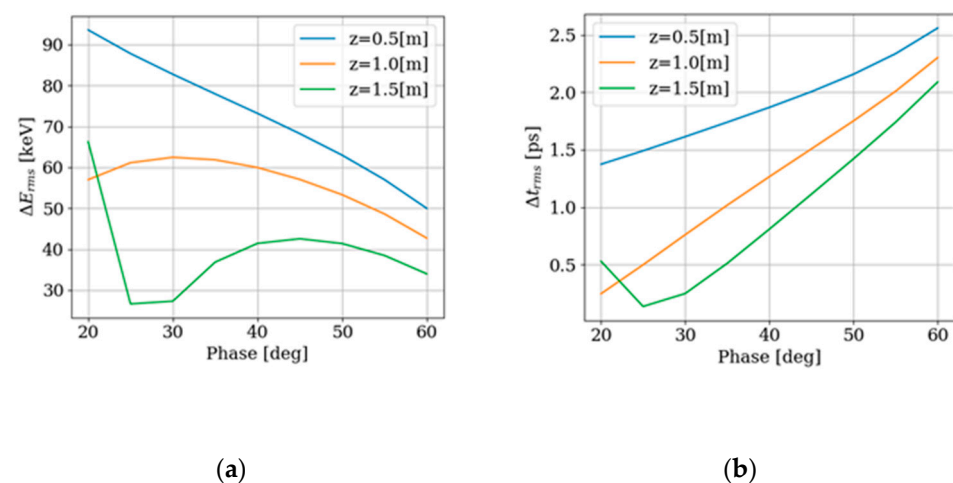
Figure 3. (**a**) Effects on energy spread; (**b**) bunch length at different z-locations along beamline versus injection phase. The design location for the entrance to the linac is 1.5 m (green).

While the hybrid gun can be operated for the purpose of maximum energy gain by detuning the temperature and injection phase, this reduces the compression and, thus, peak current, defeating its design purpose. Table 1 shows design beam parameters for an application in which peak brightness is needed, but minimized energy spread is important, such as a THz FEL.

Table 1. Electron bunch parameters for hybrid photoinjector with an application towards a THz FEL. Energy spread reported is projected, not slice. Fixed central energy of 3.9 MeV.

Charge (nC)	Emittance (mm-mrad)	Energy Spread (%)	Bunch Length (µm)	Peak Current (A)
0.1	0.6	0.19	290	41
0.25	1.1	0.26	394	76
0.5	2.0	0.33	496	120
0.75	2.9	0.38	568	158
1	3.8	0.42	626	191
2	7.5	0.55	791	303

The other advantage of this hybrid design is the propagation direction of RF power. Only a very small fraction of the RF is reflected from the standing wave structure, and most travels through and exits the gun; therefore, there is no need for an RF isolator before the gun to protect the klystron. Additionally, the spent RF power, of which only about 10% is expended in beam acceleration and pulsed heating, can then be used to power an additional accelerating section after the gun. Inserting a high-power RF phase shifter (and attenuator if needed) between the gun output and additional linac allows for phased injection and energy tuning. This is indeed the design for MITHRA, where a single 25 MW XK-5 drives the gun and a 1.5 m linac (RI Research Instruments GmbH, 51429 Bergisch Gladbach, Germany, P95861, 2856 MHz, Shunt impedance > 50 MOhm/m), which is expected to accelerate the velocity bunched beam to 30 MeV. A second 25 MW XK-5 will be used to drive a 3 m SLAC-section, increasing the energy to 80 MeV.

The hybrid gun was previously conditioned and characterized at the PEGASUS lab at UCLA, where parameters were explored with RF power of only 11.5 MW, significantly below the design of 25 MW [3]. This has the effect of lowering the beam energy as well as the chirp produced in the travelling wave section. Additionally, because the field in the standing wave section was not optimal, the charge extracted was low. Compounding this was the limited UV energy delivered by the drive laser, resulting in only 1 pC of charge for those measurements.

During characterization at MITHRA, significantly more RF power and cathode laser energy has been available. Currently, 20 MW of RF power is being delivered to the gun, with over 150 uJ of UV on the copper cathode. We have measured 250 pC of charge on a Faraday cup located approximately 2 m downstream of the cathode plane. It should be noted that an old, oxidized cathode was installed for the purpose of conditioning, due to the gun being decommissioned for an extended period, hence the low QE of ~8×10^{-6}. A new copper cathode will be installed, and laser cleaning performed prior to installing the 1.5 m linac. Laser cleaning methods learned at SLAC and used at LCLS and ASTA will be adopted at MITHRA. At ASTA, improvements were made to the method already used at LCLS, where it was found that laser energies as low as 7 µJ and increased in small steps up to <15 µJ resulted in improvement in QE from 5×10^{-6} to 5×10^{-5}, and then continued improvement to 1×10^{-4}. The laser size was kept at 40 µm rms during cleaning and the raster step size was 30 µm [8].

Using this method of laser cleaning developed at ASTA, which is considered somewhat more 'gentle' than what was traditionally used at LCLS, there was no increase in dark current from the baseline value of <100 pC. Considering the relatively low fields in the hybrid gun and adherence to the ASTA method of laser cleaning, we don't expect an increase in dark current post-cleaning of the cathode.

A CAD rendering of the low energy beamline is shown in Figure 4. A beam diagnostic station at each UHV cube is composed of a vertical "ladder" of different screens mounted on a linear translator. These locations have a YAG screen for transverse beam imaging, slits or hole arrays for emittance measurements, and a 45 degree, mirrored, metallic surface for CTR transport. The CTR emission is then extracted through a THz transparent, z-cut quartz window and transported to a Michelson-type, bunch length interferometer system (BLIS—built by Radiabeam Technologies, LLC, Santa Monica, CA 90404, USA), where the bunch length can be reconstructed from the far infrared spectrum [9,10].
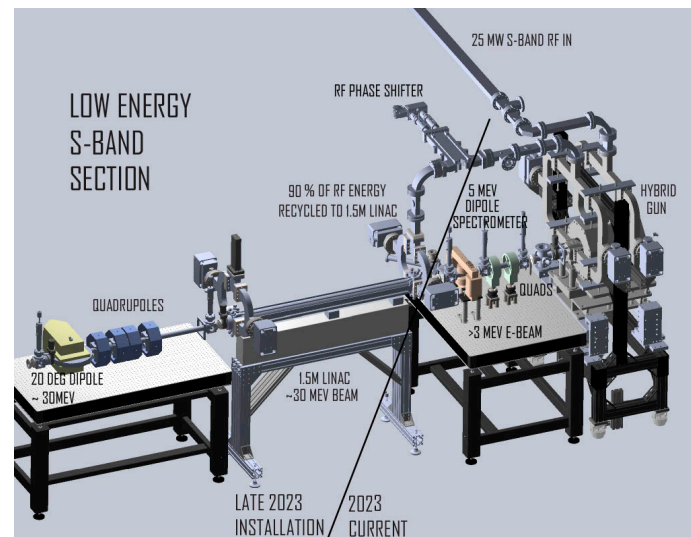
Figure 4. Three-dimensional CAD rendering of low energy (~4 MeV) beamline with future 1.5 m linac upgrade to 30 MeV.

Due to the velocity bunching of the electron bunch leaving the travelling wave section of the hybrid gun, a strong space charge force is felt due to compression, so it is desired to measure and understand the temporal evolution of the bunch as it travels down the beamline and before it is injected into the linac. Additionally, the evolution of the emittance before injection into the linac needs to be studied. This necessitates multiple diagnostic stations down the length of beamline so as to fully understand the beam dynamics before installing the linac. Shown in Figure 5 is the evolution of the beam up to the 1.5 m linac and subsequent acceleration. Parameters were optimized for the shortest bunch with 250 pC and application towards emulating space plasmas. Again, simulations were performed using GPT.

(a)   **(b)**
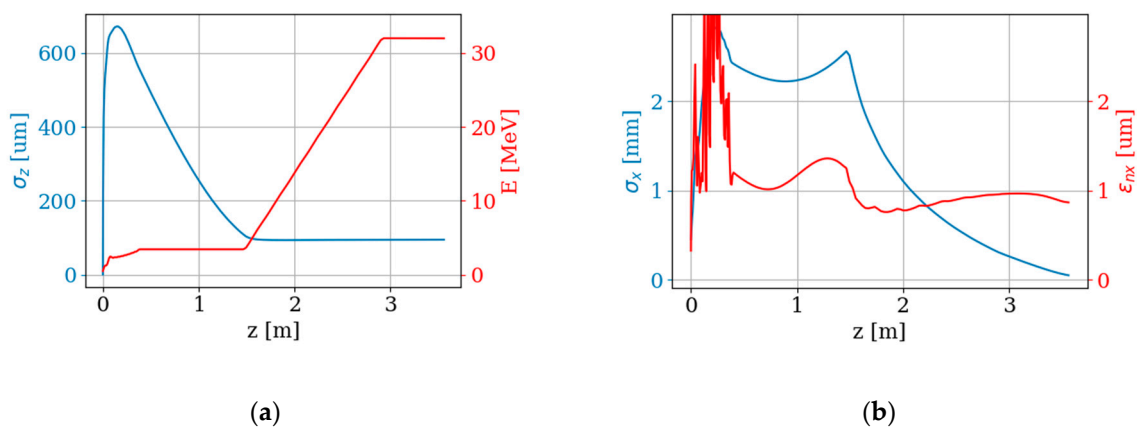
Figure 5. (**a**) Beam evolution of bunch length and energy to end of 1.5 m linac and, similarly, (**b**) transverse size and emittance. Injection into the linac occurs at 1.5 m.

Coupled with the need to measure bunch length and emittance is knowing the corresponding energy spread. The velocity bunching is dependent on the phase between the standing and travelling wave, and, hence, energy chirp gained in the travelling wave section; therefore, the resultant energy spread is an indicator of the potential for bunching. We have installed a low energy spectrometer designed for up to 5 MeV electrons for this purpose. An example of measured beam central energy and energy spread is shown in Figure 6 and additional measurements are ongoing for different parameters, including laser injection phase, gun temperature, and RF power. A summary of current electron beam and laser parameters at MITHRA is shown in Table 2.

(a)   **(b)**
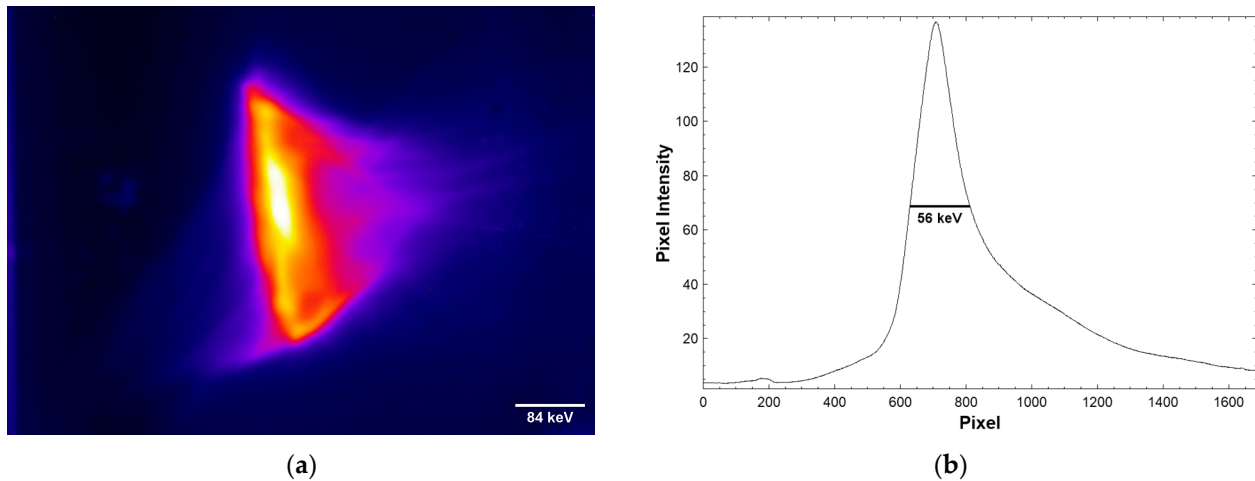
Figure 6. (**a**) Image of the 250-pC electron beam on the spectrometer screen after the 45° bend. The central energy is ~4.2 MeV; (**b**) profile of beam energy and FWHM energy spread.

Table 2. Current electron and laser parameters present at MITHRA. Beam repetition rate can be increased to 10 Hz once conditioning is complete and if the application requires it.

e-Beam	RF	Cathode Laser	Terawatt Laser
250 pC	2856 MHz	267 nm	800 nm
4.3 MeV	20 MW	150 μJ	120 mJ
56 keV (1.3%)	2.5 μs	2 ps	35 fs
1 Hz	1 Hz	10 Hz	10 Hz

3. First Experiments

It is expected that in late 2023–early 2024, the 1.5 m linac will be installed and the beam energy increased to 30 MeV. This will allow for multiple experiments and benchmarking milestones to become feasible. We will start with a range of experiments in plasma, dielectric structures, and inverse Compton scattering, reflective of the gained experience at PBPL.

3.1. Beam-Plasma Interactions

The interaction between relativistic electron beams and plasmas is of broad interest, from high field particle acceleration for future high energy physics colliders, to fundamental studies of space plasma physics. In the former case, where we access the blow-out regime of the plasma wakefield accelerator, we seek to explore two new fundamental phenomena. The first is the long-term relaxation of nonlinear plasma waves excited by the beam via ion motion and instabilities, at timescales not accessible in other labs (discussed below), and with uniquely detailed diagnostic systems. This will answer questions about the repetition frequencies usable in the PWFA. The second is the first exploration of PWFA in magnetized systems, which will shed light on cosmic acceleration processes.

In the case of near-earth space plasmas, it is of vital interest to study the phenomenon of "killer electrons" in radiation belts, to understand the genesis of auroral phenomena, and the mechanisms for precipitating very energetic electrons out of the magnetosphere, including possible remediation from pollution of the magnetosphere with energetic electrons, and fundamental wave-particle interactions. The set of experiments proposed will examine various aspects of space physics phenomena in controlled experiments in the laboratory.

3.1.1. Large Plasma Device

Among the multiple plasma sources available at MITHRA is the LArge Plasma Device (LAPD), which produces a highly magnetized, 18-m-long and 60-cm-wide plasma [11]. The LAPD, as part of the greater, NSF-funded Basic Plasma Science Facility, is located directly underneath the bunker, and we intend to build a 180-degree, vertical bend to inject the relativistic electron beam into this unique device to study the long timescale decay of wave excitation in the plasma, where sub-100 GHz electromagnetic signals would be evidence of the wave excitation and collapse. The strongly magnetized, sub-Tesla plasma also allows for studying beam head erosion control. Figure 7 shows the vertical bend into LAPD after a dogleg in the 30 MeV line.
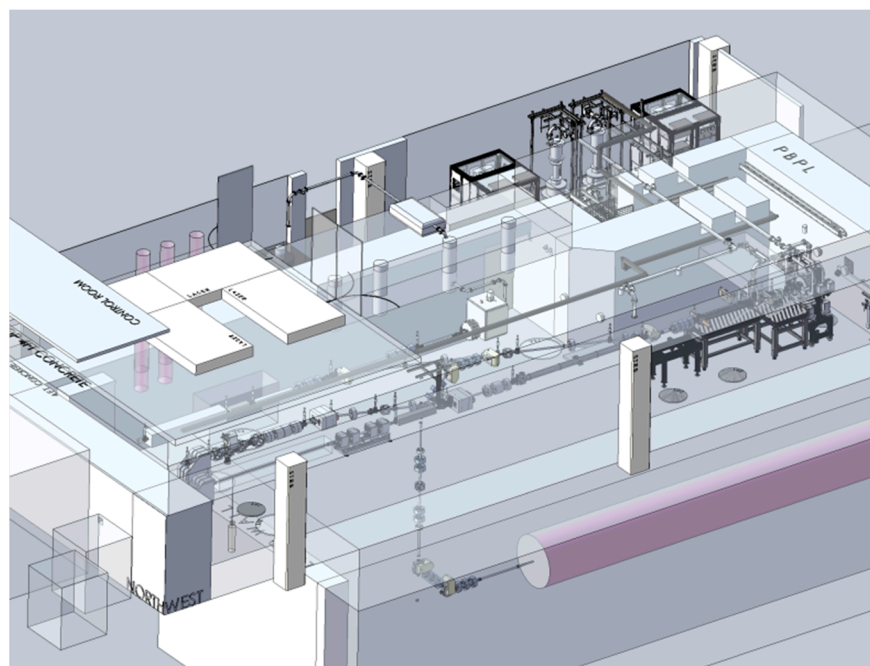
Figure 7. Three-dimensional CAD rendering of the planned 80 MeV beamline(s), including a 30 MeV dogleg and vertical bend into the Large Plasma Device bunker.

In addition to the array of probes already available to study the plasma, changes in cyclotron radiation generated by the beam could indicate variations in the strength or geometry of the magnetic fields in the plasma, providing insight into the physics of plasma confinement.

3.1.2. Space Plasma

In addition to the planned injection of the beam into the LAPD, there is interest in creating a space plasma environment which emulates the Jovian electron spectrum. Using a dense electron bunch and capillary discharge plasma currently in development, a very broad electron energy spectrum can be generated, allowing for study and testing of Jupiter-bound equipment using a terrestrial source.

Beam parameters tailored for injection into the plasma capillary are optimized for high charge density. The simulations for the beam evolution and resultant electron spectrum

after passing through the plasma have initial conditions given by: electron energy of 25 MeV, charge of 250 pC, 95 μm bunch length, 0.9 mm-mrad emittance, 16 μm spot size, and a plasma density of 1×10^{16} cm^{-3}. Fields approaching 2 GV/m are generated and experienced by the electron bunch. The results are shown in Figure 8.
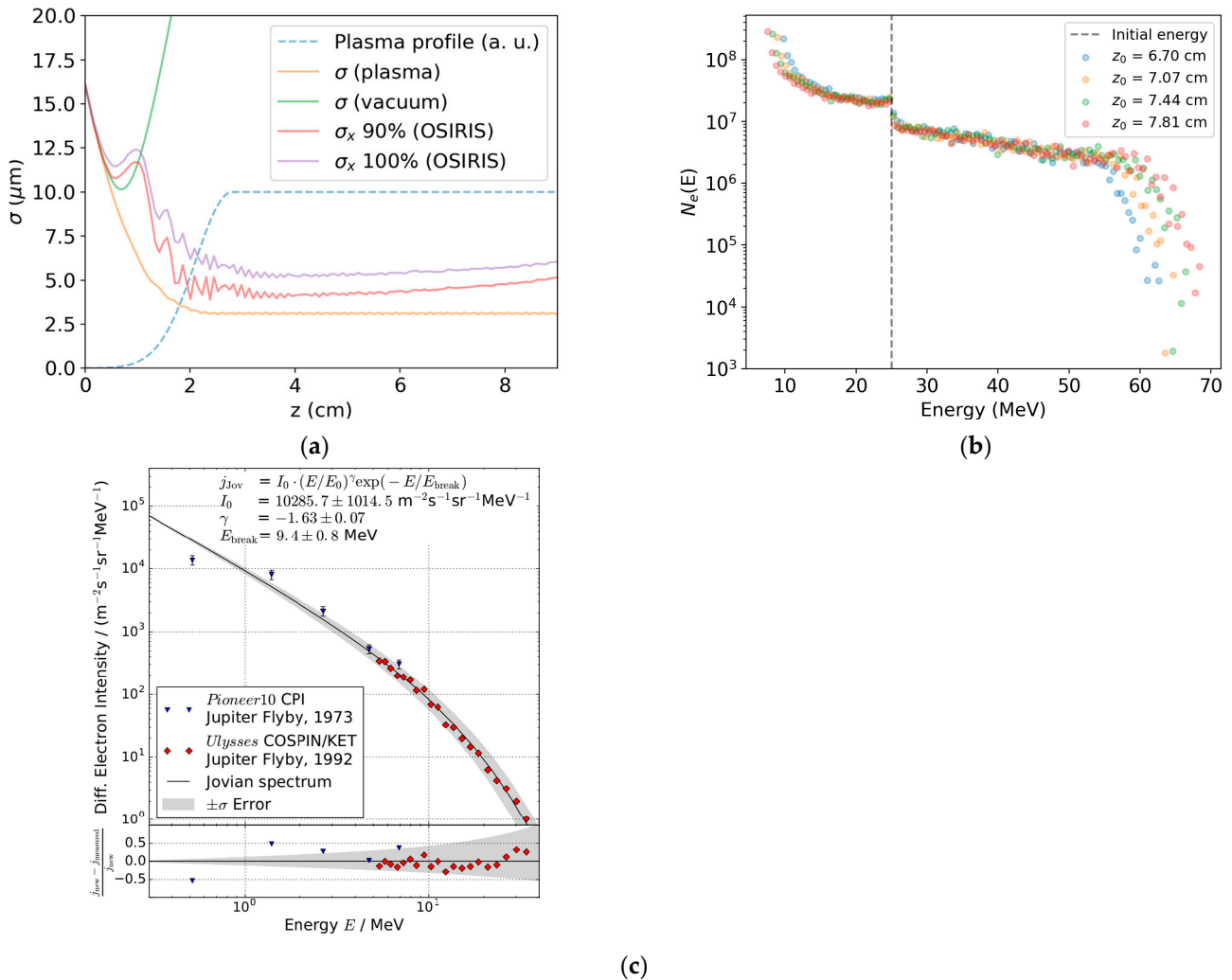
Figure 8. (**a**) Transverse evolution of beam in plasma, where σ$_x$ accounts for head erosion; (**b**) electron spectrum after traversing the plasma capillary. Dotted black line indicates the initial electron beam energy; (**c**) Jovian electron spectrum [12].

The plasma capillary is currently under development and measurements on its density profile are underway. An electron spectrometer that is capable of resolving the full energy range of electrons after traversing the plasma, from 10 to 70 MeV, is in its initial design phase.

3.2. Dielectric Wakes and THz Radiation

There is an extensive history at PBPL of successful experiments studying wakefields generated by electron beams traversing dielectric structures [13,14]. Modulation of the beam and coherent Cerenkov radiation (CCR) generated in the THz regime will be studied and applications explored, with an interest in medical applications.

Many of the THz sources that exist today are laser-based and involve nonlinear mixing in crystals to produce broadband sources. These sources have applications in spectroscopy where a scan of resonant absorption peaks is needed, but when the target absorption peak is known, it is desirable to have a frequency-matched, narrow band source of high power.

A relevant absorption peak under study in medicine occurs at 1.65 THz, which is a marker of the demethylation of DNA, an indicator of carcinogenesis [15].

An electron beam of low emittance and short bunch length, capable of traversing a small channel in a thin-walled dielectric structure, and exciting a high frequency fundamental mode of 1.65 THz, can produce the narrow bandwidth, high-power source that is needed for this application.

After an electron beam with parameters shown in Table 3 traverses an annular, fused silica-lined waveguide with inner radius of 100 μm, outer radius of 117 μm, and 1 cm length, approximately 20 μJ of THz energy is emitted with a spectrum shown in Figure 9, indicating a central frequency of 1.66 THz and bandwidth of 100 GHz. Engineering is ongoing to develop the interaction chamber and THz transport optics for delivery to experiments.

Table 3. Parameters for first proof-of-principle inverse Compton scattering source.

e-Beam	Laser	Compton X-rays
250 pC	800 nm	1×10^8 photons/s
30 MeV	120 mJ	E_{peak} = 21 keV
dE/E = 0.5%	35 fs	$\theta_{emission}$ = 17 mrad
$\sigma_{x,y}$ = 20 μm	$w_{x,y}$ = 20 μm	-
σ_z = 90 μm	Z_R = 1.6 mm	-
10 Hz	10 Hz	10 Hz
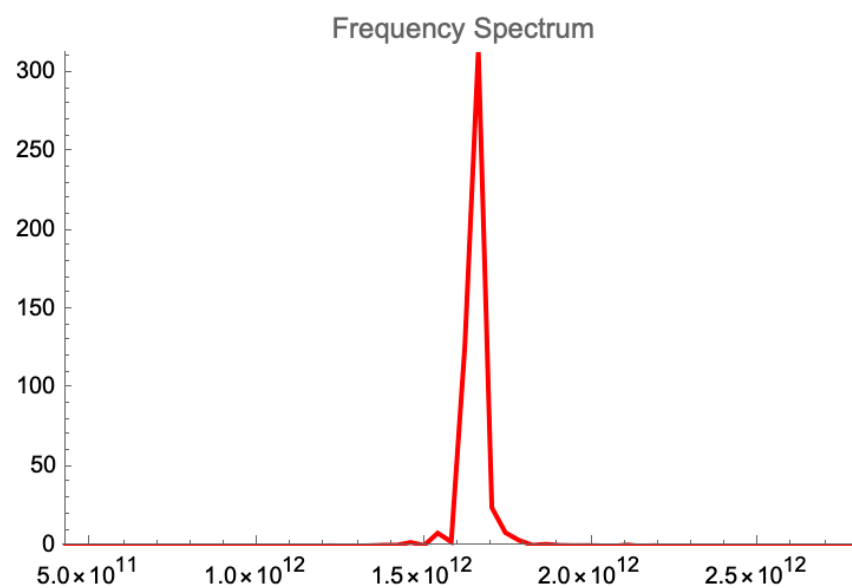
Figure 9. Spectrum of coherent Cerenkov radiation produced by the electron beam in a dielectric-lined waveguide. The central frequency is 1.66 THz with a bandwidth of 100 GHz.

3.3. Inverse Compton Scattering

The experience that PBPL has in experiments generating X-rays through inverse Compton scattering makes this a natural endeavor for the MITHRA facility [16,17]. While ICS-generated X-rays have many applications, including medicine and the study of radioisotopes, the photon energies obtainable in this beginning stage of first experiments are more suited towards other applications, including those involving cultural heritage research using X-ray absorption spectroscopy, specifically for elements with K- and L-edge absorption peaks at less than 20 keV [18]. Example parameters for the X-ray source are given in Table 3 and spectra can be seen in Figure 10.
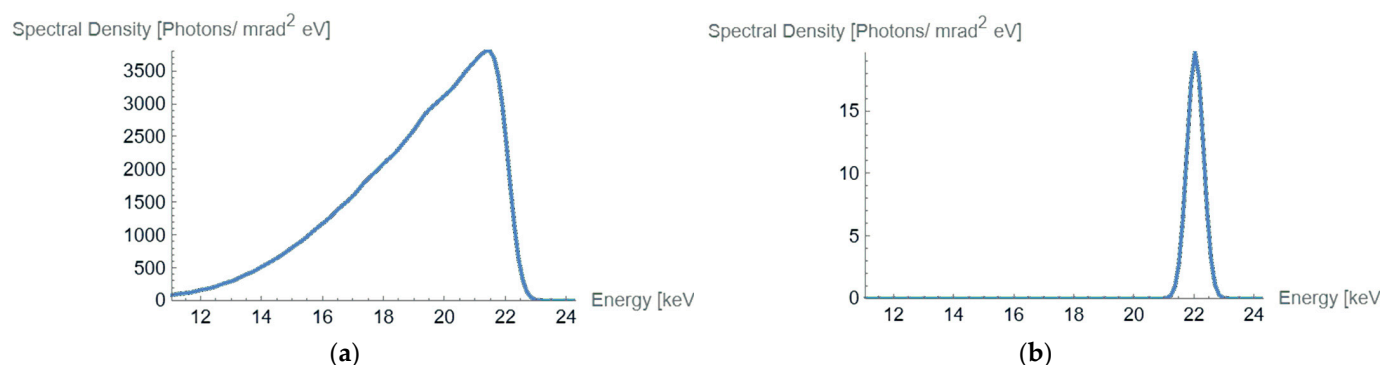
Figure 10. (**a**) ICS spectrum for the full emission angle; (**b**) 1 mrad acceptance angle.

Following installation of the terawatt laser transport line, efforts will go towards the spatial and temporal overlap of the electron and laser beams at an interaction region. Details for accomplishing overlap are not covered here, but will involve a pinhole and electro-optic sampling for synchronization. Due to the increased path length of the cathode laser pulse to reach the gun and subsequent electron propagation down the beamline, a delay line will be used for the high-power laser to compensate for the difference.

The vacuum chamber layout and infrastructure required for dielectric wakefield and ICS interactions have many similarities and should allow for relatively seamless transitions between the two.

4. Summary

The MITHRA facility at UCLA has the infrastructure necessary for research and applications in a broad range of disciplines. The high-brightness electron beam can be used for THz and X-ray radiation production, as well as advanced acceleration and basic plasma science research. A terawatt laser system expands on these capabilities and provides additional options through electron-laser interactions.

The first beam has been produced and rigorous characterization is underway, after which an upgrade to 30 MeV will be performed by installing a 1.5 m linac. This milestone will allow for multiple experiments and benchmarks to be attempted and additional applications to come into focus as capabilities become clearer.

Author Contributions: Conceptualization and Project Administration, O.W., Y.S., A.F. and J.R.; Methodology and Software, G.A., F.B., M.C., P.M., S.O., J.P. and M.Y.; Investigation, O.W., Y.S. and A.F.; Formal Analysis, A.F. and M.C.; Supervision, J.R.; Visualization and Writing, O.W. All authors have read and agreed to the published version of the manuscript.

Funding: This research was funded by U.S. DOE: DE-SC0009914, U.S. DOD: DARPA GRIT 20204571, U.S. DOE: DE-SC0020409-Cryo RF.

Data Availability Statement: The data presented in this study are available upon request from the corresponding author.

Acknowledgments: Thanks to administrative support at UCLA and technical support provided by Zoltan Lucky at STRB.

Conflicts of Interest: The authors declare no conflict of interest. The funders had no role in the design of the study; in the collection, analyses, or interpretation of data; in the writing of the manuscript; or in the decision to publish the results.

References

1. Rosenzweig, J.B.; Cahill, A. Ultra-high brightness electron beams from very-high field cryogenic radiofrequency photocathode sources. *Nucl. Instrum. Methods Phys. Res. Sect. A Accel. Spectrom. Detect. Assoc. Equip.* **2018**, *909*, 224–228. [CrossRef]
2. Lawler, G. Cyborg Beamline Development Updates. In Proceedings of the 5th North American Particle Accelerator Conference, NAPAC2022, Albuquerque, NM, USA, 7–12 August 2022. [CrossRef]

3. Fukasawa, A.; To, H.; Mahapatra, S.K.; Baumgartner, B.; Cahill, A.; Fitzmorris, K.; Li, R.; Musumeci, P.; Rosenzweig, J.B.; Spataro, B.; et al. Progress on the Hybrid Gun Project at UCLA. *Phys. Procedia* **2014**, *52*, 2–6. [CrossRef]

4. Palmer, D.T.; Wang, X.J.; Miller, R.H.; Babzien, M.; Ben-Zvi, I.; Pellegrini, C.; Sheehan, J.; Skaritka, J.; Winick, H.; Woodle, M.; et al. Emittance studies of the BNL/SLAC/UCLA 1.6 cell photocathode RF gun. In Proceedings of the 1997 Particle Accelerator Conference (Cat. No.97CH36167), Vancouver, BC, Canada, 16 May 1997; Volume 3, pp. 2687–2689. [CrossRef]

5. O'Shea, B.; Rosenzweig, J. RF Design of the UCLA/INFN Hybrid SW/TW Photoinjector. *AIP Conf. Proc.* **2006**, *877*, 873–879. [CrossRef]

6. Rosenzweig, J.B.; Valloni, A. Design and applications of an X-band hybrid photoinjector. *Nucl. Instrum. Methods Phys. Res. Sect. A Accel. Spectrom. Detect. Assoc. Equip.* **2011**, *657*, 107–113. [CrossRef]

7. Spataro, B.; Valloni, A. RF properties of a X-band hybrid photoinjector. *Nucl. Instrum. Methods Phys. Res. Sect. A Accel. Spectrom. Detect. Assoc. Equip.* **2011**, *657*, 99–106. [CrossRef]

8. Zhou, F.; Sheppard, J.C. Establishing Reliable Good Initial Quantum Efficiency and In-Situ Laser Cleaning for the Copper Cathodes in the RF Gun. 2016. SLAC-PUB-16439, Internal SLAC Publication. Available online: https://www.slac.stanford.edu/pubs/slacpubs/16250/slac-pub-16439.pdf (accessed on 10 November 2023).

9. Lai, R.; Sievers, A.J. Determination of a charged-particle-bunch shape from the coherent far infrared spectrum. *Phys. Rev. E* **1994**, *50*, R3342–R3344. [CrossRef]

10. Murokh, A.; Rosenzweig, J.B. Bunch length measurement of picosecond electron beams from a photoinjector using coherent transition radiation. *Nucl. Instrum. Methods Phys. Res. Sect. A Accel. Spectrom. Detect. Assoc. Equip.* **1998**, *410*, 452–460. [CrossRef]

11. Gekelman, W.; Pribyl, P. The upgraded Large Plasma Device, a machine for studying frontier basic plasma physics. *Rev. Sci. Instrum.* **2016**, *87*, 025105. [CrossRef]

12. Vogt, A.; Heber, B. Jovian electrons in the inner heliosphere-Proposing a new source spectrum based on 30 years of measurements. *Astron. Astrophys.* **2018**, *613*, A28. [CrossRef]

13. Cook, A.M.; Tikhoplav, R. Observation of Narrow-Band Terahertz Coherent Cherenkov Radiation from a Cylindrical Dielectric-Lined Waveguide. *Phys. Rev. Lett.* **2009**, *103*, 095003. [CrossRef]

14. Andonian, G.; Williams, O. Resonant excitation of coherent Cerenkov radiation in dielectric lined waveguides. *Appl. Phys. Lett.* **2011**, *98*, 202901. [CrossRef]

15. Son, J.-H.; Oh, S.J.; Cheon, H. Potential clinical applications of terahertz radiation. *J. Appl. Phys.* **2019**, *125*, 190901. [CrossRef]

16. O'Shea, F.H.; Williams, O. Single shot diffraction of picosecond 8.7-keV X-ray pulses. *Phys. Rev. Spec. Top.-Accel. Beams* **2012**, *15*, 020702. [CrossRef]

17. Sakai, Y.; Gadjev, I. Single shot, double differential spectral measurements of inverse Compton scattering in the nonlinear regime. *Phys. Rev. Accel. Beams* **2017**, *20*, 060701. [CrossRef]

18. Janssens, K.; Cotte, M. Using Synchrotron Radiation for Characterization of Cultural Heritage Materials. In *Synchrotron Light Sources and Free-Electron Lasers: Accelerator Physics, Instrumentation and Science Applications*; Jaeschke, E.J., Khan, S., Schneider, J.R., Hastings, J.B., Eds.; Springer International Publishing: Berlin/Heidelberg, Germany, 2020; pp. 2457–2483.